Real-time Wing Deformation Simulations for Flying Insects

Qiang Chen Jiangxi University Finance and **Economics** Nanchang, Jiangxi, P. R. China qiangchen@jxufe.edu.cn

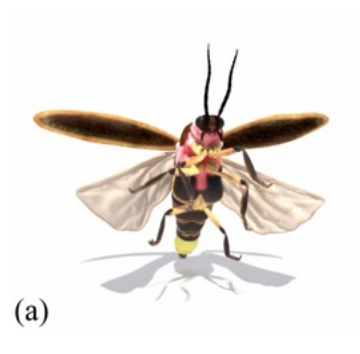
Yuming Fang[†] Jiangxi University Finance and **Economics** Nanchang, Jiangxi, P. R. China fa0001ng@e.ntu.edu.sg

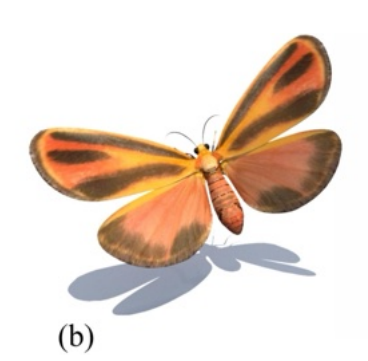
Zhigang Deng* University of Houston Houston, Texas, USA zdeng4@central.uh.edu

Tingsong Lu Yang Tong East China Jiaotong University Nanchang, Jiangxi, P. R. China lutingsong@foxmail.com tongyang@ecitu.edu.cn

Feng Li Jiangxi University Finance and **Economics** Nanchang, Jiangxi, P.R. China 2202120513@stu.jxufe.edu.cn

Yifan Zuo Jiangxi University Finance and **Economics** Nanchang, Jiangxi, P. R. China kenny0410@126.com





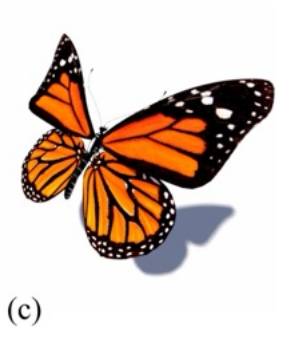


Figure 1: Our method can real-time simulate realistic wing deformations of a wide range of flying insects, including (a) fireflies, (b) painted lichen moths, and (c) monarch butterflies.

ABSTRACT

Realistic simulation of the intricate wing deformations seen in flying insects not only deepens our comprehension of insect flight mechanics but also opens up numerous applications in fields such as computer animation and virtual reality. Despite its importance, this research area has been relatively underexplored due to the complex and diverse wing structures and the intricate patterns of deformation. This paper presents an efficient skeleton-driven model specifically designed to real-time simulate realistic wing deformations across a wide range of flying insects. Our approach begins with the construction of a virtual skeleton that accurately reflects the distinct morphological characteristics of individual insect species. This skeleton serves as the foundation for the simulation of the intricate deformation wave propagation often observed in wing

Permission to make digital or hard copies of all or part of this work for personal or classroom use is granted without fee provided that copies are not made or distributed for profit or commercial advantage and that copies bear this notice and the full citation on the first page. Copyrights for components of this work owned by others than the author(s) must be honored. Abstracting with credit is permitted. To copy otherwise, or republish, to post on servers or to redistribute to lists, requires prior specific permission and/or a fee. Request permissions from permissions@acm.org.

SIGGRAPH Conference Papers '24, July 27-August 1, 2024, Denver, CO, USA © 2024 Copyright held by the owner/author(s). Publication rights licensed to ACM. ACM ISBN 979-8-4007-0525-0/24/07 https://doi.org/10.1145/3641519.3657434

†co-corresponding author

deformations. To faithfully reproduce the bending effect seen in these deformations, we introduce both internal and external forces that act on the wing joints, drawing on periodic wing-beat motion and a simplified aerodynamics model. Additionally, we utilize massspring algorithms to simulate the inherent elasticity of the wings, helping to prevent excessive twisting. Through various simulation experiments, comparisons, and user studies, we demonstrate the effectiveness, robustness, and adaptability of our model.

CCS CONCEPTS

• Computing methodologies → Physical simulation; Simulation by animation.

KEYWORDS

wing deformations, aerodynamics models, flying insects, force based simulation, deformation wave propagation

ACM Reference Format:

Qiang Chen, Zhigang Deng, Feng Li, Yuming Fang, Tingsong Lu, Yang Tong, and Yifan Zuo. 2024. Real-time Wing Deformation Simulations for Flying Insects. In Special Interest Group on Computer Graphics and Interactive Techniques Conference Conference Papers '24 (SIGGRAPH Conference Papers '24), July 27-August 1, 2024, Denver, CO, USA. ACM, New York, NY, USA, 11 pages. https://doi.org/10.1145/3641519.3657434

^{*}co-corresponding author

1 INTRODUCTION

Insect wings, characterized by their intricate structures, exhibit a wide range of deformations during flight. As highlighted in numerous biological studies [Johansson and Henningsson 2021; Young et al. 2009], these wing deformations significantly contribute to the aerodynamic efficiency of flying insects. A substantial body of experimental research has been dedicated to examining the topography and deformations of insects in free-flight [Aguayo et al. 2010; Cheng et al. 2008; Koehler et al. 2012; Young et al. 2009]. Simulating these nuanced wing deformations not only enriches our understanding of insect flight mechanics but also offers numerous applications in diverse fields such as animation, virtual reality, and entertainment.

In the realm of biological mechanics, the flight of flying insects is facilitated by the contraction and relaxation of thorax muscles [Dickinson et al. 2000] to move the wings, a process that results in considerable deformations, the result of the complex interactions between wing components [Rajabi et al. 2022; Rajabi and Gorb 2020], along the wing's chord (camber) and span (twist) during flapping flight. Despite their significance, the impacts of these deformations remain inadequately explored in existing literature [Zheng et al. 2013].

Previous studies have primarily used polygon-based methods to simulate insect wing motion during flight [Chen et al. 2022b; Dickson et al. 2006; Wilson and Albertani 2014]. However, these techniques often fall short of capturing the intricacies of wing deformations accurately. The challenge of realistically simulating these subtle deformations persist as a relatively uncharted area in computer graphics and animation research. A key aspect of this challenge is the motion initiation at the wing's leading edge, leading to a distinct wave propagation phenomenon during deformation [Wootton 1981; Wu et al. 2010]. This process begins at the wing's root, extending towards the tip (camber or longitude bending), and progresses from the leading edge to the trailing edge (twist or transverse bending), as depicted in Figure 3.

Inspired by the above challenges, we introduce a novel real-time, skeleton-driven framework designed to simulate the nuanced deformations of flying insect wings. Our methodology commences with the construction of a virtual skeleton that accurately reflects the distinct morphology of various insect species. This skeleton is crucial for emulating the complex pattern of wave propagation observed in wing deformations. To simulate the bending effects of these deformations, our model introduces a dual-force approach. Internal forces, stemming from the insect's periodic wing-beat motion driven by root muscles, are combined with external forces modeled using simplified aerodynamics principles. Additionally, our simulation employs a mass-spring algorithm to mimic the natural elasticity of insect wings.

The effectiveness and adaptability of our model are evaluated through extensive simulation experiments and comparisons. Our experiments show that our model can not only simulate the wing deformations of a wide array of flying insects, such as butterflies, moths, and fireflies, but also show its applicability to other animals. For example, we effectively simulated the wing-like motions of a freely swimming aquatic fish, demonstrating the potential of our

model's generalization beyond flying insect simulation. Figure 1 shows some example results by our approach.

The main contributions of this work can be summarized as follows:

- It introduces an effective algorithm to real-time simulate wing deformation waves, commonly observed on the wings of some flying insects.
- It introduces new force-based algorithms to efficiently emulate wing deformations in a wide range of flying insects.

The remainder of this paper is organized as follows. Section 2 provides a review of recent studies that are relevant to the presented work. A schematic overview of our methodology is delineated in Section 3. Sections 4 detail radial-shaped skeletons and the algorithm to simulate the propagation of the deformation waves on the wings. Our bending simulation algorithms, including forces computation, are presented in Section 5. Section 6 describes the simulations related to the elasticity. Our experimental results, comparisons, and user study results are presented in Section 7. Lastly, limitations of this work and potential future research directions are discussed in Section 8.

2 RELATED WORK

In this section, we briefly review recent efforts that are highly related to this work.

Experimental measure and analysis of wings. Various experimental apparatuses have been meticulously designed to quantitatively analyze the shapes, sizes, and deformations of insect wings by capturing continuous wing motion. For example, Lecuit and Le Goff [2007] explored cellular patterns and tissue-level motion in moth wings. Bai et al. [2016] studied variations in wing shapes based on digitized landmark data acquired from grasshopper wings. Salcedo et al. [2019] analyzed and identified wing sizes, contour shapes, and vein topologies in a variety of insects. Cheng et al. [2008] employed a Fourier transform method to gauge the deformations in dragonfly wings during free flight. Lehmann et al. [2011] proposed a model to measure the stiffness, elastic deformation, and energy loss of fly wings in flapping motion. Wehmann et al. [2019] designed and applied an optical apparatus to measure local deformations and stiffness distribution in flapping wings.

In addition to the above measure and analysis of living insects' wings, researchers have also examined the deformation characteristics of artificial wings [Naka and Hashimoto 2015; Van Truong et al. 2017]. Wu et al. [2010], for example, used an artificial wing to study the correlation between structural deformations and thrust using a flexible membrane. Furthermore, Finite Element Analysis (FEA) and Computational Fluid Dynamics (CFD) have been used to analyze the wake turbulence induced by wing-beats [Koehler et al. 2011].

Despite the successes of the above methods, even the most intricately designed experimental methodology cannot exhaustively measure the minutiae of wing bending. Consequently, it remains challenging to utilize such data to simulate subtle wing deformations and twisting of flying insects under a range of natural conditions.

Rigid body simulations for wing flapping motion. The simulation of wing flapping in prior studies often conceptualizes the wing as a rigid body. For example, Dickson et al. [2006] utilized periodic functions to simulate the interaction between insect wings and abdomens. Wilson and Albertani [2014] applied rigid body methods to model wing-beat motion, considering the inertia of the abdomen. To simulate the long-range flight of flying creatures, Wu and Popović [2003] implemented proportional derivative controllers for wing movements, coupled with trajectory optimization to emulate dynamic wing beats. Won et al. [2017, 2018] started with hand-crafted kinematic motions to approximate wing beats, and then applied deep reinforcement learning to refine these models, enabling the generation of more nuanced wing movements. Recently, Chen et al. [2022b] introduced a practical model to simulate butterfly flight, employing parametric maneuvering functions to generate realistic butterfly wing motion. Additionally, various models have been proposed for the simulation of insect swarms [Li et al. 2015; Wang et al. 2014; Xiang et al. 2020]. Despite these advances, a common limitation persists in these methodologies: the treatment of wing motion as rigid body dynamics. This constraint hampers their ability to authentically reproduce the dynamic deformations observable in flapping wings.

Note that certain technical components of our work may share similarity with those in the work by Chen et al. [2022b], specifically, applying aerodynamics forces to act on flying insects and periodical design to control wing motion. However, the work by Chen et al. [2022b] mainly solves parameterized maneuvering functions for butterfly flight simulation. Their model cannot handle flexible wing deformations. By contrast, our model mainly focuses on the real-time generation of realistic wing deformations, and our methodology is substantially different from Chen et al. [2022b]. Furthermore, both the vortex force and abdomen movements in Chen et al. [2022b] are not considered in our model. The main reason is that they have negligible effect on the geometric deformations of wing surfaces.

Elastic body simulations. Simulation of thin objects, represented as elastic bodies using polygon-based meshes, is a well-established technique in computer graphics [Chen et al. 2018; Choi et al. 2007]. Accurately modeling thin shells as three-dimensional elastic solids often requires fine Finite Element Method (FEM) meshes to capture global bending behaviors [Barbič and James 2005]. Cloth simulation models, aimed at generating realistic elastic objects, have also been extensively explored in the literature [Baraff and Witkin 1998; Wu et al. 2022]. Simulation of one-dimensional structures like elastic rods [Bergou et al. 2008; Spillmann and Teschner 2007] and hair strands [Selle et al. 2008] represents common applications in this domain. Moreover, the stochastic dynamics of two-dimensional fabrics, including the simulation of wrinkles and the wave dynamics of flapping flags, have been the subject of significant research [Blinn 1978; Bridson et al. 2005; Hoepffner and Naka 2011; Kavan et al. 2011; Li et al. 2022]. In addition, skeleton-based models have also been used to simulate the movements and feather deformations of a flapping bird [Ju et al. 2013].

However, it is critical to note that simulations of the wing deformations of flying insects present unique challenges. They undergo

considerable chord-wise (camber) and span-wise (twist) deformations during flapping flight, exhibiting specialized deformation characteristics. Also, wing motion typically starts at the leading edge, leading to a distinct propagation of deformation waves. Therefore, directly applying existing thin-shell models or standard cloth simulation algorithms is inadequate to capture the intricate deformations seen in insect wings.

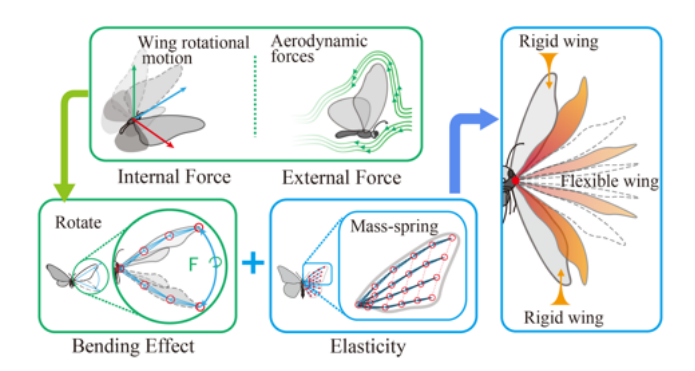


Figure 2: Schematic view of our approach

3 OVERVIEW OF OUR METHOD

Our method consists of the following main steps. First, we create a virtual skeleton for the wings, meticulously reflecting the topography. Second, based on the constructed skeleton, our algorithms simulate realistic deformations of insect wings by integrating the following modules: (i) a novel algorithm that propagates deformation waves across the wing from the leading edge to the trailing edge; (ii) simulation of the bending effect observed in insect wings, by applying forces to the skeletal joints that take into account both an internal force and an external aerodynamic force; and (iii) simulation of the elasticity in leading-edge-driven wings, facilitated by a mass-spring algorithm. As described in the above steps, our method is practical for artists to apply it in industry practice. Figure 2 illustrates the key modules in our approach.

4 DEFORMATION WAVE PROPAGATION SIMULATION

In this work, we define a complete cycle of wing flapping motion, beginning with the wing at its highest position, descending to the lowest position (downstroke), and then ascending back to the initial high position (upstroke). Concurrently, the wing undergoes sweeping and feathering motions throughout the cycle. These flapping, sweeping, and feathering motions are depicted in Figure 4. Our observations indicate that during a wing-beat cycle, encompassing flapping, sweeping, and feathering, the wing deformation predominantly initiates at the wing root and progresses towards the wing tip along the leading edge. This progression results in a phenomenon we term as *longitudinal deformation wave propagation*.

Furthermore, we observe a *transverse deformation wave propagation*, where the deformation starts at the leading edge and proceeds to the trailing edge. In this cycle, the motion commences at the leading edge and culminates at the trailing edge, eventually reverting

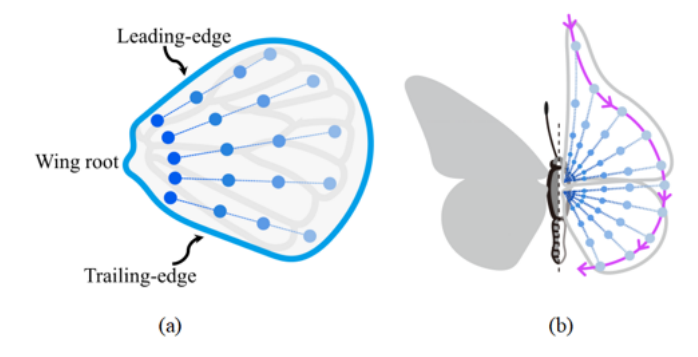


Figure 3: (a) Illustration of a radial-shaped virtual skeleton deigned for the wing and the longitudinal deformation wave propagation from the wing root to the wing tip. (b) The transverse deformation wave propagation from the leading edge to the trailing edge is driven through the chains of skeletal joints.

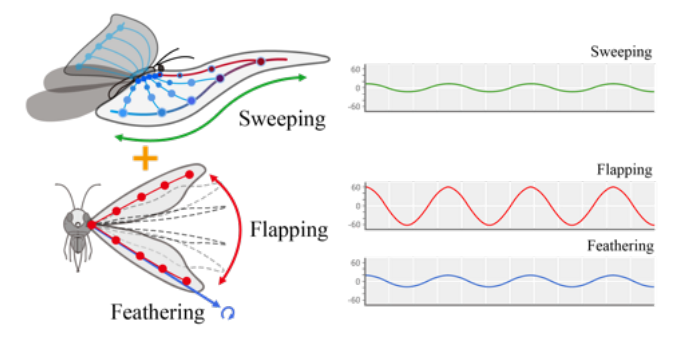


Figure 4: Illustration of wing wave motion decomposition. The wing motion of a flying insect can be decomposed into flapping, feathering, and sweeping. Each motion presents periodic features and drives the wing to deform with a wave propagation.

to the initial position. We refer to this as transverse deformation wave propagation. To simulate the transverse waves, we design radial-shaped chains of joints for each wing, as depicted in Figure 3(a) and discussed in Section 4.1. The process of the transverse deformation wave propagation is also illustrated in Figure 3(b).

Simulating deformation wave propagation in triangle mesh models presents significant challenges, particularly when replicating the complex wing beats of flying insects, which encompass three distinct rotational motions: flapping, sweeping, and feathering. In addition, the wings exhibit unique bending and elasticity characteristics during flight, further complicating the simulation process. To address these challenges, we design a hierarchical virtual skeleton embedded within the wing structure, which serves as a guideline to accurately model wing deformations (detailed Section 4.1). Building on this skeletal framework, we introduce effective algorithms designed to realistically simulate both longitudinal and transverse deformation wave propagations, as elaborated in Section 4.2.

4.1 Wing Skeleton Creation

To date, no existing solutions or guidelines have been established for the creation of virtual skeletons specifically tailored for flying insects. In this study, we introduce an empirical approach, constructing a principal chain of joints along the leading edge to mimic the arm-like motion of the wing. To accurately represent the phenomenon of deformation wave propagation in the wing, additional chains of joints are added, radiating from the wing's root to its tip.

In the manual skeleton design step, users would need to first have close-up view image(s) of the wing of a target flying insect. By respecting the topology and vein structure of specific wings, users then empirically determine the locations and the numbers of joints in the wings. In our experiments, we empirically found the number of chains should have at least three in one wing, and the number of joints in each chain should be at least three. This design is illustrated in Figure 3(a). A key feature of our method is that each chain contains an equal number of joints, thereby simplifying the process for artists and practitioners who consider to apply our approach in practice.

After the virtual skeleton design, we rig the wing mesh using the dual quaternion skinning approach [Kavan et al. 2007]. We maintain a data structure to map each joint (e.g., the i-th joint) to its influenced vertices (i.e., $\{v_j|w_{ij}\neq 0\}$, where w_{ij} denotes the skinning weight of the i-th joint on the j-th vertex v_j), and such mappings are pre-computed in the rigging process. The flying insects experimented with in this work include monarch butterfly, firefly, painted lichen moth, and fishfly. The wing shapes, triangle meshes, and skeletons of these insects are illustrated in Figure 7.

In the following Section 4.2, we will describe how we simulate the macro-level deformation wave propagation phenomenon based on the cycles of wing flapping motion. In Sections 5 and 6, we will describe how we simulate micro-level deformations on the wings, including bending and elasticity.

4.2 Longitudinal and Transverse Wave Simulation

Longitudinal Wave Simulation. Since a wave ends when a motion cycle is completed, one solution for longitudinal wave simulation (cycle motion) is to use a cosine function, without considering the wave speed v, described as follows:

$$W(t) = A\cos(2\pi f t + \varphi),\tag{1}$$

where W is a waveform function, A is amplitude, f is frequency, and φ is phase shift. By complying with Equation 1, each chain of joints with three instantaneous rotational motion (flapping, sweeping, and feathering) is used to drive the longitudinal wave motion.

Transverse Wave Simulation. During transverse deformation wave propagation, the leading edge first initiates flapping through the principal chain of joints, and the remaining chains of joints follow in sequence, each with a distinct delay. Assuming that there are n chains of joints in the wing, the delay time $\hat{t}(\mathbf{r}_i)$ of the i-th chain of joints relative to the principal chain of joints during a cycle can be calculated as follows:

$$\hat{t}(\mathbf{r}_i) = \frac{1}{2f} \frac{\|\mathbf{r}_i - \mathbf{r}_1\|}{\|\mathbf{r}_n - \mathbf{r}_1\|},\tag{2}$$

where \mathbf{r}_1 , \mathbf{r}_i , and \mathbf{r}_n represent the 3D positions of the root joints of the first (principal), the *i*-th, and the *n*-th chains of joints, respectively.

To this end, by integrating the longitudinal and transverse wave propagations, our model drives each chain of joints as follows:

$$W_i(t, \mathbf{r}_i) = A \cos \left(2\pi f \left(\left(t - \hat{t}(\mathbf{r}_i) \right) \Pi \left(t - \hat{t}(\mathbf{r}_i) \right) \right) + \varphi \right), \quad (3)$$

where $\Pi(\cdot)$ is a Heaviside function, and it is 0 for $t-\hat{t}(\mathbf{r}_i) < 0$, which indicates the i-th chain of joints is still waiting for the initiation of flapping motion. Note that $t-\hat{t}(\mathbf{r}_i)$ could be a negative value, while relative time is not allowed to be negative; thus, we introduce a Heaviside function $\Pi(\cdot)$ to prevent it.

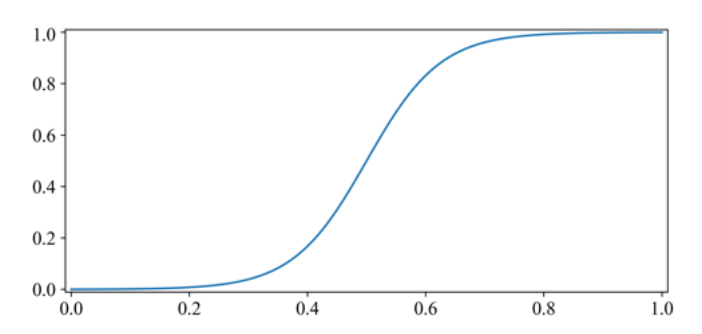


Figure 5: Plotting of the slope shape function $s(\mathbf{u}) = 1/\left(1 + e^{-16(|\mathbf{u}|/|\mathbf{u}^{max}| - \frac{1}{2})}\right)$. The X-axis denotes the magnitude of the velocity \mathbf{u} divided by the maximum velocity \mathbf{u}^{max} of the flying insect.

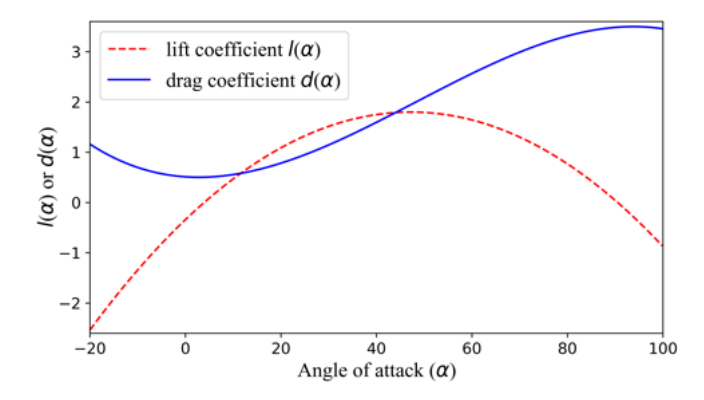


Figure 6: Correlation between the wing's local angle of attack α and the coefficients $l(\alpha)$ and $d(\alpha)$. The lift coefficient function (red curve): $-0.00095953\alpha^2 + 0.090635\alpha - 0.34182$, and the drag coefficient function (blue curve): $-0.0000079518\alpha^3 + 0.0011527\alpha^2 + 0.0063148\alpha + 0.51127$.

5 BENDING SIMULATIONS

We design internal and external forces that are applied onto the joints to simulate bending effects on the wings. Besides the gravity, the forces considered in this work also include:

- The **internal force** (described in Section 5.1), \mathbf{F}^{in} , is generated from the rotational motion of the wing. The internal force is applied onto the joints in the skeleton.
- The **external force**, **F**^{ex}, which is essentially a simplified aerodynamic force (described in Section 5.2), computed for each triangle of the wing mesh.

To rotate the joints to simulate the bending effect, we compute torques based on the aforementioned forces. The torque τ_i for the i-th joint is calculated as follows:

$$\tau_i = \hat{\mathbf{r}}_i \times (\mathbf{F}_i^{in} + \sum_j \frac{\mathbf{F}_{ij}^{ex}}{3} + m_i \mathbf{g}), \tag{4}$$

where \mathbf{F}_i^{in} is the internal force applied to the *i*-th joint; \mathbf{F}_{ij}^{ex} is the resultant external force applied to the *j*-th vertex that is influenced by the *i*-th joint in the skinning model; $\hat{\mathbf{r}}_i$ denotes a vector from the *i*-th joint, \mathbf{r}_i , to the wing root; \mathbf{g} is the gravitational acceleration; and m_i is the mass for the *i*-th joint. In this work, the mass of a joint is computed as the $\{w_{ij}\}$ weighted sum of the masses of the triangles that are influenced by this specific joint (that is, $w_{ij} > 0$ for all the three vertices of the influenced triangle). Also, we treat the mass of the entire wing as one unit mass, and then compute the mass of the *i*-th triangle according to the ratio of its area to the entire wing area in the initial state.

5.1 Internal Forces

From a biological perspective, flying insects drive their wings through the muscles at the root of the wing [Johansson and Henningsson 2021; Young et al. 2009]. But few, if any, existing studies provide quantitative or even qualitative models for computing such muscle forces. In this work, we assume we can utilize rotational motion to inversely compute the corresponding internal forces. Specifically, the internal force of the *i*-th joint is computed from the wing's harmonic oscillations (Equation 1), with the dynamical amplitude and frequency as follows:

$$T_{i,t}^{\star} = m_i \mathbf{a}_t^{\star}$$

$$= -2m_i (2\pi f^{\star}(\mathbf{u}_t))^2 A^{\star}(\mathbf{u}_t) \cos(2\pi f^{\star}(\mathbf{u}_t)t) \mathbf{e}^{\star}, \qquad (5)$$
where $\star \in \{\text{flapping, feathering, sweeping}\},$

where $\mathbf{F}_{i,t}^{\star}$ is the internal force of the *i*-th joint for one of the rotational motion types at time t; m_i is the mass of the *i*-th joint; \mathbf{e}^{\star} is the rotational direction of the wing at the start time; $f^{\star}(\mathbf{u}_t)$ and $A^{\star}(\mathbf{u}_t)$ are frequency and amplitude functions, respectively; \mathbf{u}_t is the velocity of the flying insect at time t. Here, we ignore the phase shifts because the three types of cycle motion start at the same time

Following the work of [Chen et al. 2022b], we vary the values of frequency and amplitude at each cycle according to the velocity of the insect body \mathbf{u} . Within each cycle of wing motion, the frequency and amplitude (i.e., $f^*(\mathbf{u})$ and $A^*(\mathbf{u})$) are fixed, but they can only be changed at the start of the next cycle. Furthermore, based on our observations and the analysis of a publicly available butterfly motion capture dataset [Chen et al. 2022a], flying insects have a larger amplitude of wing motion during the take-off or climbing process than other scenarios. In addition, flying insects typically have a higher range of wing-beat angles when their bodies are

Table 1: The maximum value of amplitude MAX_a^{\star} about the flapping, feathering, and sweeping of the simulated insects. Note that these values may not be the same as the biological measurements of real insects; instead, they are mainly used for the generation of plausible visual effects.

Name	Flapping [deg]	Feathering [deg]	Sweeping [deg]
Monarch	120	24	36
Firefly	156	78	0
Fishfly	120	24	0
Painted lichen moth	126	37	37

not horizontal, i.e., AoA (angle of attack) $>0^{\circ}$, than the horizontal case [Dorsett 1962]. To this end, we design the following two functions to dynamically compute the frequency and amplitude:

$$f^{\star}(\mathbf{u}_{t_0}) = \begin{cases} max\{MAX_f * s(\mathbf{u}_{t_0}), MAX_f * 0.85\}, & AoA > \frac{\pi}{6} \\ MAX_f * s(\mathbf{u}_{t_0}), & \text{else} \end{cases}$$
(6)

and

$$A^{\star}(\mathbf{u}_{t_0}) = \begin{cases} max\{MAX_a^{\star}s(\mathbf{u}_{t_0}), MAX_a^{\star}*0.85\}, & AoA > \frac{\pi}{6} \\ MAX_a^{\star}s(\mathbf{u}_{t_0}), & \text{else} \end{cases}$$
(7)

where $\star \in \{$ flapping, feathering, sweeping $\}$, \mathbf{u}_{t_0} denotes the velocity of the insect body at the start of each motion cycle, MAX_f is the maximum value of the frequency, which is set to 11 Hz as suggested in existing biological studies [Davenport 1994; Kang et al. 2018]. The maximum values of the amplitude MAX_a^{\star} , for different flying insects are listed in Table 1. Also, as shown in Figure 5, $s(\mathbf{u})$ is a slope shape function.

Finally, we can obtain the internal force $\mathbf{F}_{i,t}^{in}$ for the *i*-th joint at time *t* in each cycle as follows:

$$\mathbf{F}_{i,t}^{in} = \sum_{\star \in \{\text{flapping, feathering, sweeping}\}} \mathbf{F}_{i,t}^{\star}. \tag{8}$$

5.2 External Forces

According to the quasi-steady state aerodynamics theory [Ellington 1984], flying insects' flapping motion can generate aerodynamics lift force and drag force. In our model, we treat aerodynamics as an external force that influences wing deformations. Inspired by previous studies of bird flapping simulations [Ju et al. 2013; Wu and Popović 2003], we compute the aerodynamics force as follows:

$$\mathbf{F}_{i,l} = \frac{1}{2} \rho s_i \|\mathbf{V}\|^2 l(\alpha), \quad \text{and} \quad \mathbf{F}_{i,d} = \frac{1}{2} \rho s_i \|\mathbf{V}\|^2 d(\alpha), \quad (9)$$

where $\mathbf{F}_{i,l}$ and $\mathbf{F}_{i,d}$ are the lift force and the drag force for the i-th triangle, respectively; ρ is an air density constant; s_i is the area of the i-th triangle; and \mathbf{V} is the air velocity over the wing's surface. If there is no wind, \mathbf{V} can be treated as the triangle's velocity. The coefficients $l(\alpha)$ and $d(\alpha)$ are determined by the wing's local angle of attack (i.e., the triangle's angle of attack), α , which can be computed as follows:

$$\alpha = \arctan(\frac{\|\mathbf{V}_{\mathbf{n}}\|}{\|\mathbf{V}_{\mathbf{t}}\|}),\tag{10}$$

where V_n and V_t are the components of the air velocity along the normal of the wing surface and along the tangent direction (i.e., the vector of base-to-tip), respectively. Inspired by the work of [Dickinson et al. 1999], we introduce empirical Lift/Drag coefficient functions. Figure 6 plots the relation between the wing's local angle of attack α and the coefficients $l(\alpha)$ and $d(\alpha)$.

The resultant aerodynamics force then can be calculated as follows:

$$\mathbf{F}^{ex} = \sum_{i} (\mathbf{F}_{i,l} + \mathbf{F}_{i,d}). \tag{11}$$

The computed aerodynamic force is equally applied to the three vertices of the triangle (that is, each of the three vertices receives 1/3 of this specific triangle-based external force). Thus, each vertex has a resultant force accumulated from its adjacent triangles. Finally, the external force applied to the *i*-th joint is calculated as the skinning-weighted sum of the external forces on its influenced vertices: $F_i^{ex} = \sum_j w_{ij}.F_{ij}^{ex}$, where F_{ij}^{ex} denotes the calculated external force on the *j*-th vertex that has a skinning weight $w_{ij} > 0$ from the *i*-th joint.

6 ELASTICITY SIMULATION

Our method described above can generate rotational motion for the joints, simulating the bending effects. Furthermore, we also simulate the elasticity of the wing using a mass-spring based algorithm.

Based on the Hooke's law, we design an energy function as follows:

$$E(\mathbf{r}) = \frac{1}{2} k_e (\|\mathbf{r}_i - \mathbf{r}_j\| - L)^2, \tag{12}$$

where \mathbf{r}_i and \mathbf{r}_j are the positions of two adjacent joints (e.g., the i-th joint and the j-th joint), k_e is the elasticity coefficient, L is the rest distance between the i-th joint and the j-th joint. To this end, the spring force from this energy function generated for the i-th joint and the j-th joint are denoted as $\mathbf{f}_i = \nabla_i E$ and $\mathbf{f}_j = -\nabla_j E$, respectively.

To achieve the stability, we apply the implicit numerical integration [Baraff and Witkin 1998] to update the joint's linear velocity \mathbf{v} and position \mathbf{r} . Here, we assume that the spring force $\mathbf{f}(\mathbf{r}^{t_{k+1}})$ is holonomic, i.e., depending on the position \mathbf{r} only, we update the joint's linear velocity \mathbf{v} and position \mathbf{r} as follows:

$$\begin{cases}
\mathbf{r}^{t_{k+1}} = \mathbf{r}^{t_k} + \Delta t \mathbf{v}^{t_k} + \Delta t^2 \mathbf{M}^{-1} \mathbf{f}(\mathbf{r}^{t_{k+1}}), \\
\mathbf{v}^{t_{k+1}} = (\mathbf{r}^{t_k} - \mathbf{r}^t) / \Delta t,
\end{cases} (13)$$

where **M** is the mass matrix. Since Equation (13) is an implicit representation of $\mathbf{r}^{t_{k+1}}$, the computation of $\mathbf{r}^{t_{k+1}}$ is equivalent to solving an optimization problem as follows:

$$\mathbf{r}^{t_{k+1}} = \operatorname{argmin} F(\mathbf{r}), \tag{14}$$

for

$$F(\mathbf{r}) = \frac{1}{2\Delta t^2} \|\mathbf{r} - \mathbf{r}^{t_k} - \Delta t \mathbf{v}^{t_k}\|_{\mathbf{M}}^2 + E(\mathbf{r}), \tag{15}$$

where $E(\mathbf{r})$ is the energy function described in Equation (12). A Newton-Raphson method is used to solve the above optimization problem.

Table 2: The values of the elasticity parameter used in our experiments, the number of triangles in the wing mesh, and the simulation FPS. The simulation time step is 0.02.

Name	Elasticity k_e	# of triangles of the wing mesh	Simulation FPS
Monarch	1	4192	100
Firefly	2	12568	172
Fishfly	0.5	1210	160
Painted lichen moth	1.8	1648	150

7 RESULTS AND EVALUATIONS

We implemented our approach in Unity 3D using C# language, and we ran all our experiments on an off-the-shelf PC with Intel(R) Xeon(R) W-1290P CPU and 64G memory. To evaluate the effectiveness of our model, we created several flying insect 3D models, including two types of butterflies, a firefly, a fishfly, and a painted lichen moth (shown in Figure 7). The firefly, painted lichen moth, and fishfly are modeled according to the video from the Evolutionary Biology & Behavior Research Lab at the North Carolina Museum of Natural Sciences & North Carolina State University. Furthermore, we applied the flight simulation model in [Chen et al. 2022b] to generate dynamic fight trajectories for wing deformation examinations. The empirically used values for the elasticity parameters in our method are summarized in Table 2.

We describe our experimental results and comparisons in Section 7.1, and present our user study results in Section 7.2. For animations of our simulation results, please refer to the enclosed supplemental demo video.

7.1 Simulation Results and Comparisons

The wing deformation of a monarch butterfly. The fore-wings and hind-wings can be simply treated as a whole because it has synchronous flapping motion [Dudley 2002]. Figure 8 as well as the demo video shows a monarch butterfly with wing deformations during free flight. The simulated monarch butterfly by our approach can exhibit wing deformation waves, which propagate from the leading edge to the opposite side.

The wing deformation of a swallow-tail butterfly. Unlike the monarch butterfly, the fore-wings and hind-wings of a swallow-tail butterfly move with different flapping amplitudes, i.e., its flying mainly relies on the fore-wings. As shown in Figure 9, the simulated swallow-tail butterfly demonstrates the intricate elasticity of its wings.

#1 Comparison with a real-world monarch butterfly. In this comparison experiment, we simulated the wing deformations of a monarch butterfly in flight, and compared it with a real-world monarch butterfly video clip. As shown in Figure 10, the simulated wing deformations of the monarch butterfly, especially the deformation wave propagation effect, are similar to those of the real butterfly.

#2 Comparison with a real-world firefly. The wings of a firefly are relatively small, compared to its body. The wings of the firefly,

with transparent cell membranes, can exhibit flag-like deformations during flight. Figure 11 shows the comparison between a simulated firefly and a real-world firefly video clip. As shown in this comparison, the simulated firefly by our approach has realistic flag-like wing deformations.

#3 Comparison with a real-world painted lichen moth. The wing motion of a painted lichen moth is similar to that of a monarch butterfly. But the wings of the painted lichen moth can display more softness during free flight. For example, its wing tips nearly deform into cup-shapes, which can help to improve the flight efficiency during take-off [Johansson and Henningsson 2021]. In our experiment, we simulated the wing deformations of the painted lichen moth by tuning the elasticity parameters in our model. Our simulation results, as shown in Figure 12 and the demo video, demonstrate that our method can simulate insect wings with various elasticities.

#4 Comparison with a real-world fishfly. A fishfly with four long wings can fly with a high efficiency [Davenport 1994]. Usually, the wing-beat frequency of the fishfly is similar to that of a butterfly, i.e., 11Hz. In our experiment, we simulated the flag-like wing deformation of the fishfly and compared it with a real-world fishfly video clip. As shown in Figure 13, the simulated wings of the fishfly have realistic deformations as the real-world fishfly.

Results of different elasticity parameter values. Our model can be used to simulate different wing deformations by tuning the values of key parameters, e.g., elasticity. In this comparison, we simulated the wing deformations of a fishfly with different elasticity values. The comparison results are presented in Figure 14.

Comparisons with previous approaches. We also compared our method with one of recent butterfly flight simulation approaches in [Chen et al. 2022b]. However, the work of [Chen et al. 2022b] does not simulate the detailed wing deformations although it can achieve plausible butterfly wing-body interactions. For a fair comparison, we simulated the wing-body motion with a butterfly by our approach, and directly compared the wing deformation with the method in [Chen et al. 2022b] using the four insects in this study. Visual comparisons are shown in the supplemental demovideo.

Results of fish fin motion. Not limited to flying insects, we also applied our model on marine fish for a realistic simulation of fin motion to test its applicability to other animals. As shown in Figure 16 and the demo video, a simulated snailfish flaps its major fins, which is driven by our model, exhibiting realistic fin motion with deformation wave propagation. Note that flying insects are applied with lift/drag forces according to the aerodynamics theory, while the fish in our example is applied with similar lift and drag forces in the water. The lift and drag forces share the same functions when applied in the air or water but with different coefficients.

7.2 User Study

Although there exist wing deformation measurement experiments in biology field, the methods in existing biology literature generally divide an insect wing into patches and then gauge the patches' deformation to find max/min twists [Koehler et al. 2012; Rajabi et al. 2016]. Therefore, it is difficult for us to perform direct quantitative

comparisons between our method and existing biological study results. Also, since it is technically infeasible to acquire the ground-truth deformations of the flying insects studied in this work during their natural flights, we cannot perform quantitative evaluations on our simulation results with respect to the ground-truth. Instead, we conducted a user study to compare the simulation results by three different approaches: (I) the state of the art butterfly motion approach [Chen et al. 2022b] that is most related to our work, (II) our approach without the deformation wave propagation component, and (III) our approach. We chose the "paired comparison" evaluation scheme [Ledda et al. 2005; Ma and Deng 2009] for our user study, because, by selecting the perceptually better one between two visual stimuli (a pair), participants can avoid to make forced, inaccurate perception decisions, e.g., assign a subjective and quantitative rating to each stimulus.

We used the above three different approaches to simulate the same four flying insects (i.e., monarch butterfly, firefly, painted lichen moth, and fishfly, as described in Section 7.1), and generated a total of 12 stimuli. Then, we formed 12 pairs (e.g., (I) vs. (II), (II) vs. (III), and (III) vs. (I)) for our user study. The left/right positioning in these pairs was randomized.

A total of 40 student volunteers from a university campus participated in our user study: 8 females and 32 males; their ages range from 20 to 30 with the average age = 24.2; and all have their majors in science and engineering but are agnostic in computer animation or simulation.

Considering that most people probably never had a chance to closely watch the dynamic motion of flying insects in their daily lives, before our user study, we first showed them some Internet video clips that contain high-fidelity, close-up views of the compared flying insects, so that they can get familiar with those flying insects to a certain extent. During the study, participants can watch the two animation clips in a pair unlimited times before they selected the more realistic one between the two.

Based on the user votes obtained, we summarize the user votes in Figure 15. Our approach (method III) received significantly more votes than the other two methods in this comparison. To quantify the statistical significance of the results, we performed a two-tailed independent one-sample t-test and calculated the p-value for each row in Figure 15. As shown in this figure, our approach (method III) is statistically significantly better than our approach without deformation wave propagation (method II), while the latter is significantly better than the existing approach in [Chen et al. 2022b] (method I).

8 DISCUSSION AND CONCLUSION

In this paper we present a real-time framework to effectively simulate realistic wing deformations of flying insects, based on bioinspired, hierarchical radial-shaped skeletons. Besides simulating the deformation wave propagation phenomenon that is commonly observed on insect wings, our method can also effectively simulate the nuanced bending and elasticity effects of flying insect wings through an introduced dual-force model. Through many simulation experiments, comparisons, and user studies, we demonstrate the efficacy and robustness of our approach to simulate a variety of flying insects. However, we acknowledge our method may not be

scientifically or physically correct. The objective of this work is the design of an efficient and practical method to simulate visually plausible wing deformations for some flying insects as well as its potential applications for other animals with similar wing structures.

Our current approach can generate encouraging results, but it has the following limitations:

- Currently, we manually design the skeletons for flying insects. The skeleton design does not consider precise functions of the vein networks in the wings.
- Due to the difficulty of obtaining ground-truth motion data, we are unable to calibrate the parameters in our model or perform quantitative evaluations. Instead, our current approach has to use empirically specified parameter values.

As a future work, we plan to apply machine learning methods to extract the network of veins from 2D wing images. Based on the wing venation topology, a more accurate virtual skeleton could be created. Furthermore, an improved wing surface that respects the wing venation topology would generate more smooth and accurate wing deformations. In addition, our model can potentially be extended to support aerodynamic analysis, for example, visualization of laminar and vortex flow triggered by flexible wing flapping [Koehler et al. 2011].

ACKNOWLEDGMENTS

The authors would like to thank Dr. Huamin Wang for providing early discussion on the simulation algorithm. Qiang Chen was supported in part by the National Natural Science Foundation of China (Grant No. 62262024), and Science Foundation of the Jiangxi Province of China (Grant No. 20232BAB202023). Yang Tong was supported in part by Scientific Research Project of Education Department of Jiangxi Province (Grant No. GJJ2200641). Yuming Fang was supported in part by National Natural Science Foundation of China (Grant No. 62441203 and 62132006), and Science Foundation of the Jiangxi Province of China (Grant No. 20223AEI91002). Yifang Zuo was supported in part by the National Natural Science Foundation of China (Grant No. 62271237) and Excellent Youth Foundation of Jiangxi Scientific Committee (Grant No. 20224ACB212005). Zhigang Deng was in part supported by US NSF IIS-2005430.

REFERENCES

Daniel D Aguayo, Fernando Mendoza Santoyo, H Manuel, Manuel D Salas-Araiza, Cristian Caloca-Mendez, and David Asael Gutierrez Hernandez. 2010. Insect wing deformation measurements using high speed digital holographic interferometry. Optics express 18, 6 (2010), 5661–5667.

Yi Bai, Jia-Jia Dong, De-Long Guan, Juan-Ying Xie, and Sheng-Quan Xu. 2016. Geo-graphic variation in wing size and shape of the grasshopper Trilophidia annulata (Orthoptera: Oedipodidae): morphological trait variations follow an ecogeographical rule. Scientific reports 6, 1 (2016), 1–15.

David Baraff and Andrew Witkin. 1998. Large steps in cloth simulation. In *Proceedings* of the 25th annual conference on Computer graphics and interactive techniques. 43–54. Jernej Barbič and Doug L James. 2005. Real-time subspace integration for St. Venant-Kirchhoff deformable models. *ACM transactions on graphics (TOG)* 24, 3 (2005), 982–900

Miklós Bergou, Max Wardetzky, Stephen Robinson, Basile Audoly, and Eitan Grinspun. 2008. Discrete elastic rods. In ACM SIGGRAPH 2008 papers. 1–12.

James F Blinn. 1978. Simulation of wrinkled surfaces. ACM SIGGRAPH computer graphics 12, 3 (1978), 286–292.

Robert Bridson, Sebastian Marino, and Ronald Fedkiw. 2005. Simulation of clothing with folds and wrinkles. In ACM SIGGRAPH 2005 Courses. 3–es.

- Hsiao-Yu Chen, Arnav Sastry, Wim M van Rees, and Etienne Vouga. 2018. Physical simulation of environmentally induced thin shell deformation. ACM Transactions on Graphics (TOG) 37, 4 (2018), 1–13.
- Qiang Chen, Tingsong Lu, Yang Tong, Yuming Fang, and Zhigang Deng. 2022a. A Practical Method for Butterfly Motion Capture. In Proceedings of the 15th ACM SIGGRAPH Conference on Motion, Interaction and Games (Guanajuato, Mexico) (MIG '22). Association for Computing Machinery, New York, NY, USA, Article 8, 9 pages.
- Qiang Chen, Tingsong Lu, Yang Tong, Guoliang Luo, Xiaogang Jin, and Zhigang Deng. 2022b. A Practical Model for Realistic Butterfly Flight Simulation. ACM Transactions on Graphics (TOG) 41, 3 (2022), 1–12.
- Peng Cheng, Jinsong Hu, Guofeng Zhang, Lei Hou, Boqin Xu, and Xiaoping Wu. 2008. Deformation measurements of dragonfly's wings in free flight by using Windowed Fourier Transform. Optics and lasers in engineering 46, 2 (2008), 157–161.
- Min Gyu Choi, Seung Yong Woo, and Hyeong-Seok Ko. 2007. Real-time simulation of thin shells. In Computer Graphics Forum, Vol. 26. Wiley Online Library, 349–354.
- John Davenport. 1994. How and why do flying fish fly? Reviews in Fish Biology and Fisheries 4, 2 (1994), 184–214.
- Michael H Dickinson, Claire T Farley, Robert J Full, MAR Koehl, Rodger Kram, and Steven Lehman. 2000. How animals move: an integrative view. *science* 288, 5463 (2000), 100–106.
- Michael H Dickinson, Fritz-Olaf Lehmann, and Sanjay P Sane. 1999. Wing rotation and the aerodynamic basis of insect flight. *Science* 284, 5422 (1999), 1954–1960.
- William Dickson, Andrew Straw, Christian Poelma, and Michael Dickinson. 2006. An integrative model of insect flight control. In 44th AIAA Aerospace Sciences Meeting and Exhibit. 34.
- DA Dorsett. 1962. Preparation for flight by hawk-moths. *Journal of Experimental Biology* 39, 4 (1962), 579–588.
- Robert Dudley. 2002. The biomechanics of insect flight: form, function, evolution. Princeton University Press.
- Charles Porter Ellington. 1984. The aerodynamics of hovering insect flight. I. The quasi-steady analysis. Philosophical Transactions of the Royal Society of London. B, Biological Sciences 305. 1122 (1984). 1–15.
- Jérôme Hœpffner and Yoshitsugu Naka. 2011. Oblique waves lift the flapping flag. Physical Review Letters 107, 19 (2011), 194502.
- LC Johansson and P Henningsson. 2021. Butterflies fly using efficient propulsive clap mechanism owing to flexible wings. *Journal of the Royal Society Interface* 18, 174 (2021), 20200854.
- Eunjung Ju, Jungdam Won, Jehee Lee, Byungkuk Choi, Junyong Noh, and Min Gyu Choi. 2013. Data-driven control of flapping flight. ACM Transactions on Graphics (TOG) 32, 5 (2013), 1–12.
- Chang-kwon Kang, Jacob Cranford, Madhu K. Sridhar, Deepa Kodali, David Brian Landrum, and Nathan Slegers. 2018. Experimental Characterization of a Butterfly in Climbing Flight. AIAA Journal 56, 1 (2018), 15–24.
- Ladislav Kavan, Steven Collins, Jiří Žára, and Carol O'Sullivan. 2007. Skinning with dual quaternions. In *Proceedings of the 2007 symposium on Interactive 3D graphics and games.* 39–46.
- Ladislav Kavan, Dan Gerszewski, Adam W Bargteil, and Peter-Pike Sloan. 2011. Physicsinspired upsampling for cloth simulation in games. In ACM SIGGRAPH 2011 papers.
- Christopher Koehler, Zongxian Liang, Zachary Gaston, Hui Wan, and Haibo Dong. 2012. 3D reconstruction and analysis of wing deformation in free-flying dragonflies. Journal of Experimental Biology 215, 17 (2012), 3018–3027.
- Christopher Koehler, Thomas Wischgoll, Haibo Dong, and Zachary Gaston. 2011. Vortex visualization in ultra low Reynolds number insect flight. IEEE transactions on visualization and computer graphics 17, 12 (2011), 2071–2079.
- Thomas Lecuit and Loïc Le Goff. 2007. Orchestrating size and shape during morphogenesis. *Nature* 450, 7167 (2007), 189–192.
- Patrick Ledda, Alan Chalmers, Tom Troscianko, and Helge Seetzen. 2005. Evaluation of tone mapping operators using a high dynamic range display. ACM Transactions on Graphics (TOG) 24, 3 (2005), 640–648.
- Fritz-Olaf Lehmann, Stanislav Gorb, Nazri Nasir, and Peter Schützner. 2011. Elastic deformation and energy loss of flapping fly wings. Journal of Experimental Biology 214, 17 (2011), 2949–2961.
- Weizi Li, David Wolinski, Julien Pettré, and Ming C. Lin. 2015. Biologically-inspired visual simulation of insect swarms. In Computer Graphics Forum, Vol. 34. Wiley Online Library, 425–434.
- Yifei Li, Tao Du, Kui Wu, Jie Xu, and Wojciech Matusik. 2022. DiffCloth: Differentiable cloth simulation with dry frictional contact. ACM Transactions on Graphics (TOG) 42, 1 (2022), 1–20.
- Xiaohan Ma and Zhigang Deng. 2009. Natural eye motion synthesis by modeling gaze-head coupling. In 2009 IEEE Virtual Reality Conference. IEEE, 143–150.
- Hisayoshi Naka and Hiromu Hashimoto. 2015. Effects of deformation and vibration characteristics of wings on flapping flight. Mechanical Engineering Journal 2, 1 (2015), 14–00262.
- Hamed Rajabi, Sepehr H Eraghi, Ali Khaheshi, Arman Toofani, Cherryl Hunt, and Robin J Wootton. 2022. An insect-inspired asymmetric hinge in a double-layer membrane. Proceedings of the National Academy of Sciences 119, 45 (2022), e2211861119.

- H Rajabi and SN Gorb. 2020. How do dragonfly wings work? A brief guide to functional roles of wing structural components. *International journal of odonatology* 23, 1 (2020), 23–30.
- Hamed Rajabi, M Rezasefat, A Darvizeh, J-H Dirks, SH Eshghi, A Shafiei, T Mirzababaie Mostofi, and Stas N Gorb. 2016. A comparative study of the effects of constructional elements on the mechanical behaviour of dragonfly wings. Applied Physics A 122 (2016) 1–13
- Mary K Salcedo, Jordan Hoffmann, Seth Donoughe, and L Mahadevan. 2019. Computational analysis of size, shape and structure of insect wings. *Biology Open* 8, 10 (2019), bio040774.
- Andrew Selle, Michael Lentine, and Ronald Fedkiw. 2008. A mass spring model for hair simulation. In ACM SIGGRAPH 2008 papers. 1–11.
- Jonas Spillmann and Matthias Teschner. 2007. CoRdE: Cosserat rod elements for the dynamic simulation of one-dimensional elastic objects. In Proceedings of the 2007 ACM SIGGRAPH/Eurographics symposium on Computer animation. 63–72.
- Tien Van Truong, Quoc-Viet Nguyen, and Heow Pueh Lee. 2017. Bio-inspired flexible flapping wings with elastic deformation. Aerospace 4, 3 (2017), 37.
- Xinjie Wang, Xiaogang Jin, Zhigang Deng, and Linling Zhou. 2014. Inherent noise-aware insect swarm simulation. In Computer Graphics Forum, Vol. 33. Wiley Online Library, 51–62.
- Henja-Niniane Wehmann, Lars Heepe, Stanislav N Gorb, Thomas Engels, and Fritz-Olaf Lehmann. 2019. Local deformation and stiffness distribution in fly wings. Biology open 8, 1 (2019), bio038299.
- Tyler Wilson and Roberto Albertani. 2014. Wing-flapping and abdomen actuation optimization for hovering in the butterfly Idea leuconoe. In 52nd Aerospace Sciences Meeting. 0009.
- Jungdam Won, Jongho Park, Kwanyu Kim, and Jehee Lee. 2017. How to train your dragon: example-guided control of flapping flight. ACM Transactions on Graphics (TOG) 36, 6 (2017), 1–13.
- Jungdam Won, Jungnam Park, and Jehee Lee. 2018. Aerobatics control of flying creatures via self-regulated learning. ACM Transactions on Graphics (TOG) 37, 6 (2018), 1–10.
- Robin J Wootton. 1981. Support and deformability in insect wings. Journal of Zoology 193, 4 (1981), 447–468.
- Botao Wu, Zhendong Wang, and Huamin Wang. 2022. A GPU-Based Multilevel Additive Schwarz Preconditioner for Cloth and Deformable Body Simulation. ACM Trans. Graph. 41, 4, Article 63 (jul 2022), 14 pages.
- Jia-chi Wu and Zoran Popović. 2003. Realistic modeling of bird flight animations. ACM Transactions on Graphics (TOG) 22, 3 (2003), 888–895.
- Pin Wu, Peter Ifju, and Bret Stanford. 2010. Flapping wing structural deformation and thrust correlation study with flexible membrane wings. AIAA journal 48, 9 (2010), 2111–2122.
- Wei Xiang, Xinran Yao, He Wang, and Xiaogang Jin. 2020. FASTSWARM: A data-driven framework for real-time flying insect swarm simulation. Computer Animation and Virtual Worlds 31, 4-5 (2020), e1957.
- John Young, Simon M Walker, Richard J Bomphrey, Graham K Taylor, and Adrian LR Thomas. 2009. Details of insect wing design and deformation enhance aerodynamic function and flight efficiency. Science 325, 5947 (2009), 1549–1552.
- Lingxiao Zheng, Tyson L Hedrick, and Rajat Mittal. 2013. Time-varying wing-twist improves aerodynamic efficiency of forward flight in butterflies. *PloS one* 8, 1 (2013), e53060.

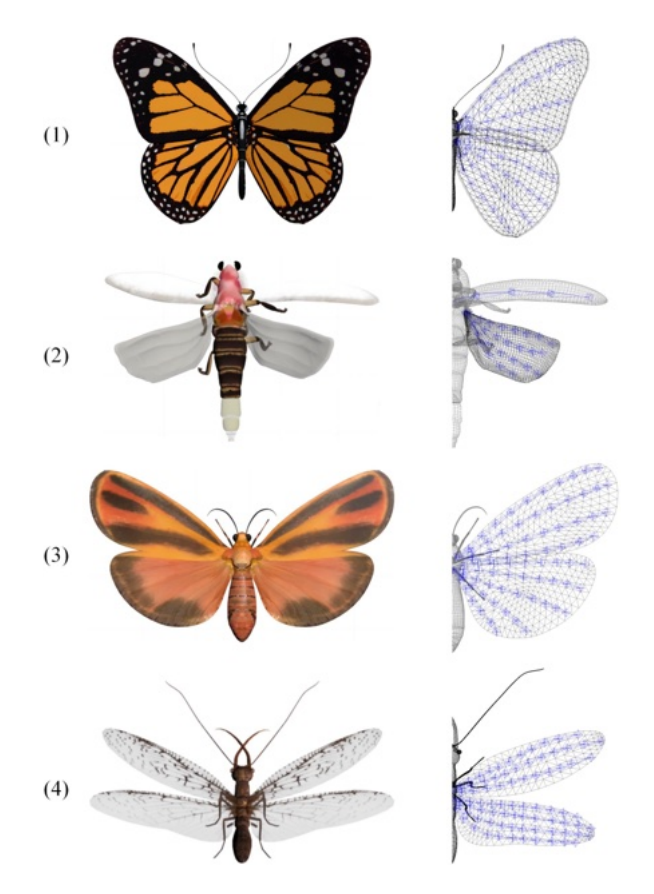


Figure 7: The constructed 3D flying insects include: (1) monarch butterfly, (2) firefly, (3) painted lichen moth, and (4) fishfly. Wing meshes and the designed skeletons are shown on the right.



Figure 8: A simulated monarch butterfly during free flight. The wing deformation waves propagate from the leading edge to the trailing edge. The deformed wings are highlighted with red arrows.



Figure 9: The wing deformations of a simulated swallowtail butterfly presents special elasticity during flight. The deformed wings are highlighted with red arrows.



Figure 10: The comparison of a real-world monarch butterfly (a) and a simulated monarch butterfly by our method. The monarch butterfly endeavor to flap wings during the climbing process and thus exhibit intricate wing deformations.



Figure 11: Comparison between a real-world firefly video clip (a) and a simulated firefly by our approach (b). The simulated wing deformations of the firefly have a flag-like deformation motion with intricate elasticity, which is similar to the real one.



Figure 12: Comparison between a real-world painted lichen moth (a) and a simulated painted lichen month by our method (b). The simulated wing tips nearly deform into cupshapes, which is similar to the real-world painted lichen moth.



Figure 13: Comparison of a real-world fishfly (a) and a simulated fishfly by our method (b). The wing deformations of the simulated fishfly exhibit intricate elasticity, which is similar to the real one.

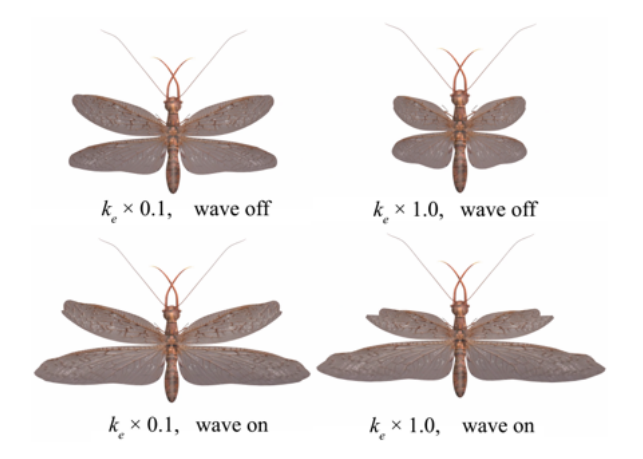


Figure 14: Comparison of the wing deformations of a fishfly, with different values of elasticity. "Wave on/off" indicates whether our deformation wave propagation algorithm is turned on or off. Results of different elastic parameter values are also compared.

Wing deformation simulation						
p<0.001 (III) Our model	152	8	(I) Chen et al' 2022b			
p<0.001 (III) Our model	144	16	(II) Our model without deformation wave			
p<0.001 (II) Our model without deformation wave	136	24	(I) Chen et al' 2022b			

Figure 15: The aggregated user voting result. The black box indicates the total number of votes for the method III - our model, the gray box indicates the total number of votes for the method II - our model without deformation wave propagation, and the white box indicates the total number of votes for the method I - the method in [Chen et al. 2022b]. All the computed *p*-values are smaller than 0.001 according to a two-tailed independent one-sample t-test.



Figure 16: Our method can simulate the fin flapping of a snailfish, with deformation wave propagation.